PFC/JA-88-47

Gyrotron Powered Standing Wave Electromagnetic Wiggler Experiment

T.S.Chu, B.G.Danly, R.Temkin

Plasma Fusion Center
Massachusetts Institute of Technology
Cambridge, MA 02139

December 1988

This work was supported by U.S. DOE Contract DE-AC03-86SF16498

Gyrotron Powered Standing Wave Electromagnetic Wiggler Experiment

Abstract

Experimental results on a gyrotron powered standing wave electromagnetic wiggler are presented. The gyrotron interaction cavity and the standing wave storage cavity are designed as a single unit. The gyrotron was operated at a high field intensity and short interaction length regime. The operating mode is the TE_{13} mode at 129.5 GHz. A value of normalized vector potential of the wiggler field of 0.0057 is obtained. The experimental results indicate that higher wiggler field strenghts should be feasible with higher power electron beams; such an advance would make possible the development of compact, low voltage, near IR FELs.

1. Introduction

The use of a high frequency electromagnetic wave as the wiggler for a free electron laser (FEL) has received increasing attention during the past decade.[1-5] The reasons are: 1) the ability to use short wavelength electromagnetic wave as the wiggler, 2) the transverse field inhomogeneity of the electromagnetic wiggler can be made small compared with that of a comparable magnetostatic wiggler. A short wavelength wiggler reduces the requirement on beam energy for a given lasing frequency. Lower beam energy can result in a compact system. Recently, the use of cyclotron resonance devices, such as the gyrotron, to power the electromagnetic(EM) wiggler field of a FEL has been proposed and analyzed.[6-8] The use of gyrotron-powered electromagnetic (GEM) wigglers and high quality electron beams of relatively low energy ($< 8MeV$) appear promising for operation of compact FEL's in the infrared to visible region of the spectrum . Such electron beams are now being obtained with photocathode injectors [9] and microwave guns [10].

In this paper, we report the experimental results on a GEM wiggler. There is no electron beam for FEL interaction in the experiments reported here. We are concerned only with the demonstration of a gyrotron-powered electromagnetic wiggler. The outline for this paper is as follows. A brief review of the mechanism of GEM wiggler FEL will be given first. Then, the design of the experiment is elaborated. Also, we describe the setup of the experiment and diagnostic equipment used. Finally, the data and results of the experiments are presented.

2. GEM Wiggler FEL

The advantages of EM wiggler FEL's have led to the proposal of several novel configurations. One such configuration is the one-beam two-stage FEL [1-5], where a magnetostatic (MS) wiggler is used in the first stage to generate the EM wiggler in the second. The configuration of GEM wiggler FEL requires two electron beams. A relatively low energy beam (50 - 200 kV) is used to operate a millimeter wave source , such as a gyrotron or a cyclotron autoresonance maser (CARM), while another beam is used to operate the FEL.

The use of a gyrotron for the first stage is made possible by the recent progress in gyrotron oscillators. [11] Gyrotrons are capable of producing high power at high frequency with high efficiency. In addition, the CARM capable of high peak power is being developed

[12,13]. In the configuration proposed here and elsewhere [6,7,8], the power generated in the first stage, gyrotron or CARM interaction region, would propagate through the second stage, the FEL interaction region, either as a travelling wave in a waveguide or a standing wave in a high Q resonator. High Q resonator is appropriate for use with gyrotrons. The high Q is required for reaching a wiggler field strength high enough for reasonable FEL gain. A schematic diagram of the standing wave GEM wiggler FEL is shown in Fig.1. This is the configuration which was investigated experimentally.

The principle of the operation of GEM wiggler FEL has been analyzed in [7,8]. For $a_w^2 \ll 1$, the gain of the GEM wiggler FEL operating in the low gain Compton regime scales as a_w^2. The normalized vector potential of the wiggler field is a_w ($a_w = eB_w/mck_{\|}$) . Therefore, determination of how a_w depends on source power, frequency, cavity Q, and wiggler cavity mode is very important in the design of GEM wiggler FEL. Although in principle the GEM wiggler can operate as either travelling wave in a waveguide or standing wave in a resonator, we operated in the standing wave configuration because it is more suitable for lower power operation. In this configuration, we have

$$a_w = 0.262((\nu_{1n}^2 - 1)J_1^2(\nu_{1n}))^{-1/2}\frac{k_\perp}{k}(\frac{QP}{\omega d})^{1/2} \qquad (1)$$

All parameter dimensions are in MKS units. Q is the total quality factor of the cavity; P, the wiggler source power; d, the FEL interaction length; ω, the angular frequency of the gyrotron; k, the wavevector; $k_\perp$, the perpendicular wavevector in the FEL interaction region; ν_{1n}, the nth zero of J_1', the derivative of Bessel function of the first kind . One notices that a_w scales as the square root of the QP product. With other parameters fixed, a 1 MW gyrotron and a cavity with a Q of 5000 would give the same a_w as a 0.2 MW gyrotron and a cavity with Q of 25000.

We digress here to point out that for a given a_w, EM wiggler would require half of the magnetic field, B_w, of MS wiggler. Moreover, the wavelength of the MS wiggler is required to be half of that of EM wiggler. This is because $a_w = eB_w/mc^2k_{\|}$ for an EM wiggler and $a_w = eB_w/mc^2k_w$ for a MS wiggler. By definition, $k_w = k + k_{\|}$. For $k_{\|} \approx k$, $\lambda_w = \lambda/2$. For a given a_w, the product of magnetic field and wavelength has to be the same for both EM and MS wiggler. Hence, the magnetic field strength for MS wiggler has to be doubled

to compensate for the factor of one half in wavelength. Table 1 compares EM and MS wigglers at different values of a_w.

3. Design of Experiment

The main component that needs to be designed in these experiments is the cavity. The cavity actually consists of two major sections. A schematic diagram of the cavity is shown in Fig.2. The first straight section is the gyrotron interaction region. This is referred to as the gyrotron cavity. To the left, it is tapered down to cut off for the operating mode. To the right, it is tapered up to another straight section, which is refered to as the FEL interaction region or the FEL cavity. To create a standing wave field in the FEL region, another down taper is employed. In order to measure the signal, the downtaper is close to but not at cutoff. The final uptaper is to provide a gradual transition between cavity and output waveguide. The design started with the set of given parameters of the electron gun [14] which was available for this experiment. These parameters are a gun voltage V of 65 kV, a beam current I of 5 A, a pitch α ($\beta_\perp/\beta_\parallel$) of 1.5. With these given parameters, the operating mode is chosen based on the strongest coupling between field and beam [15]. A typical gyrotron gun, known as a magnetron injection gun (MIG), produces an annular beam. In order to have good coupling between beam and field, the beam are placed at one of the radial maxima of the RF field. We would also like to operate in a TE_{1n} mode because the rf field of these modes is peaked on axis; this is essential for FEL interaction, where the high voltage electron beam is on axis. Based on these considerations, the TE_{13} mode was chosen. The beam was located at the second radial maximum of the field.

The gyrotron interaction length is determined based on the consideration of efficiency. Gyrotron interaction efficiency can be parameterized by normalized field strength F, normalized gyrotron interaction length μ ,and normalized current parameter I [16,17,18].

$$F = \frac{E_0}{B_0}\beta_{\perp 0}^{n-4}\left(\frac{n^{n-1}}{n!2^{n-1}}\right)J_{m\pm n}(k_\perp R_e) \tag{2}$$

$$\mu = \pi\frac{\beta_{\perp o}^2 L}{\beta_{\parallel o}\lambda} \tag{3}$$

$$I = 0.238 \times 10^{-3}(\frac{Q_T I_a}{\gamma_o})\beta_{\perp o}^{2(n-3)}(\frac{\lambda}{L})(\frac{n^n}{2^n n!})^2 \frac{J_{m\pm n}^2(k_\perp R_e)}{(\nu_{mp}^2 - m^2)J_m^2(\nu_{mp})} \tag{4}$$

Here, R_e is the beam radius, n, the harmonic number, L, the gyrotron interaction length, $k_\perp$, the perpendicular wavevector in the gyrotron cavity, ν_{mp}, the pth zero of J'_m, $\beta_{\perp o}$, the normalized initial perpendicular electron velocity, $\beta_{\|o}$, the normalized intial parallel electron velocity, I_a, the beam current. The efficiency for a range of F and μ has been previously calculated [16,17,18]. For the GEM wiggler, the normalized wiggler field strength a_w can be related to F by

$$a_w = \frac{\beta_{\perp o}^3}{\mid J_{1\pm n}(k_{\perp 1}R_e) \mid} \frac{k_{\perp 1}}{k_{\perp 2}} \frac{F}{4} \tag{5}$$

This relation results from the assumption that coupling between the gyrotron cavity and FEL cavity is strong (small reflection coefficient). At equilibrium, the power generated in region one, the gyrotron region, can be set equal to the power circulating in the FEL cavity, designated as region two. $k_{\perp 1}$ is the perpendicular wavevector in region 1, and $k_{\perp 2}$, region 2. n is the harmonic number. Since we are working with fundamental mode, n equals 1. For high a_w, one would like to operate at high F. In order to maintain high efficiency operation, the cavity is designed with a small μ.

The above considerations give a rough estimate of the various dimensions of the cavity. The actual design of cavity is carried out using a modified version of the NRL cavity field solver code CAVRF [19]. After some iterations and adjustment of dimensions, a design is obtained. The final field profile and cavity geometry is shown in Fig.3. The Q calculated is the diffractive Q, Q_d. The total Q is

$$\frac{1}{Q} = \frac{1}{Q_d} + \frac{1}{Q_{ohm}} \tag{6}$$

The ohmic Q is given by

$$Q_{ohm} = \frac{\omega W}{P_d} \tag{7}$$

where ω is the resonant frequency, W, the stored energy, P_d, the dissipated power. The energy stored in the cavity is obtained by integrating the energy density over the volume

of the cavity:

$$W = \int_v \frac{\epsilon}{2} \mid E \mid^2 dv = \int_v \frac{\mu}{2} \mid H \mid^2 dv \tag{8}$$

where $\mid E \mid$ and $\mid H \mid$ are the peak values of the field intensities. The power loss in the cavity can be evaluated by integrating the power density over the inner surface of the cavity.

$$P_d = \frac{R_s}{2} \int_s \mid H_t \mid^2 da \tag{9}$$

where H_t is the peak value of the tangential magnetic intensity and R_s is the surface resistance of the cavity. Then Q_{ohm} can be written as

$$Q_{ohm} = \frac{\omega\epsilon \int_v \mid E \mid^2 dv}{R_s \int_s \mid H_t \mid^2 da} \tag{10}$$

The above expression can be analytically integrated in r and θ. By using the field profile calculated by CAVRF, we can numerically integrate in z to get Q_{ohm}.

Design of a simple cavity with both gyrotron and FEL interaction regions has been carried out.In addition, the cavity region where the FEL wiggler field is stored is designed so that $k_{\parallel}$ / k $\approx$ 0.9 and L = 10λ, where L is cavity length. High diffractive Q is obtained for the unit. The designed parameters for the gyrotron operation and the a_w expected is summarized in Table 2. Fig.4 is a picture of the cavity.

4. Experiment

The schematic of the experiment setup is shown in Fig.5. The main field is provided by a water cooled Bitter magnet capable of producing field up to 10 Tesla. The magnetic field profile over the entire cavity is shown in Fig.6. The DC axial magnetic field is almost constant over the gyrotron section of the cavity, but it has dropped by twenty percent at the other end of the cavity. The drop in field minimizes the chance for the straight output section to act as a gyrotron cavity. A pair of auxiliary coils is used to adjust the field at the cathode of the electron gun. This is useful in optimizing the gyrotron operation.

The diagnostics used in the GEM wiggler experiment include power, frequency and mode content measurement. Power measurements were made using a thermopile calorimeter [20]. Far field patterns were obtain by scanning with a microwave diode. Frequency measurements were made with a heterodyne mixer system [21,22] and a Hughes wavemeter.

The first step in the experiment was the alignment of the cavity. This was done by eliminating any current, termed body current, which is intercepted on the cavity. A zero body current guarantees the beam clear through the entire cavity. In addition, a set of position dials were used to center the beam with respect to the cavity. After aligning the cavity, we scanned the magnetic field from 4 to 6 Tesla and detected all the signals within this range by monitoring the diode signal on the oscilloscope. For each signal, its frequency was first measured with the wavemeter. Then, the mixer system was used to measure each frequency more accurately. The mixer system is a heterodyne receiver which detects the intermediate frequency(IF) generated by mixing the incoming RF signal with a harmonic of the signal generated by the local oscillator. The IF signal is amplified and passed through a surface acoustic wave device, which is a linear dispersive delay line with transit time proportional to frequency. Passing the IF signal through the SAW filter will separate the signal into it's constituent Fourier components. For a properly gated signal the SAW output will be the Fourier transform of the IF. Provided the bandwidth of the LO signal is much less than the bandwidth of the RF, the IF spectrum is equivalent to the shifted RF spectrum. Fig. 7 shows the RF pulse for the 129.596 GHz signal. Its SAW (surface acoustic wave) signal is shown in Fig.8.

By comparing the measured frequencies with the calculated frequencies of CAVRF we can identify the operating mode corresponding to the various signals. Table.3 shows the identified modes. The 129.5 GHz signal is identified to be the TE_{13} mode, which has calculated eigenfrequency of 129.169 GHz, closest to the measured frequency. The 134 GHz signal can not be identified. At this point, we can only speculate that it is a high order axial mode. In addition, we have measured the minimum starting current of the 129.5 GHz signal and found $I_{start} = 0.3A$ at 5.14 Tesla. The calculated minimum starting current [23] for the TE_{13} mode is 0.34 A. The minimum starting current for the TE_{71} mode with an calculated eigenfrequency of 130.631 GHz is 0.6 A, which is twice as big as the measured starting current.

The far field pattern of the signals were also measured. The measured pattern of the TE_{13} mode differs from the theoretical patterns expected from an open circular waveguide [24]. This indicates the presence of mode conversion in the output signal. After the

gyrotron mode is generated in the interaction region, it is coupled into the FEL cavity, which is designed to trap the majority of the RF power. A small portion of the signal is allowed to leak out for measurement purposes. The outgoing signal has to propagate through a region with a long uptaper, which provides the transition from the cavity to the output waveguide. The tapered regions are likely to cause conversion to other modes. Hence, the presence of mode conversion is not unexpected. Although mode conversion is present in the output signal, the extent of conversion in the traped signal can not be ascertained. An alternative method has to be used to measured the mode content inside the cavity.

To determine the normalized vector potential of the wiggler field, a_w, we must measure both the power of the gyrotron mode and the total Q of the cavity. The power of the TE_{13} mode was measured using a thermoelectric calorimeter. The total Q of the cavity was measured using the setup shown in Fig.9 [25]. The measurement was made by sweeping an IMPATT diode over a range of frequency, about 2 GHz, and displaying the detected spectrum on an oscilloscope. At the resonance frequency of the cavity mode, the signal of the IMPATT diode is coupled into the cavity and a dip appears in the standing wave pattern. Since our particular IMPATT diode is only tunable in the range of 135-144 GHz, we were not able to directly measure the total Q of the TE_{13} at 130 GHz. Instead, we measured the total Q of the TE_{42} cavity mode at 141 GHz. The Q of the TE_{13} mode is then interpolated from the 141 GHz data using the ratio of experimental Q to theoretical Q of TE_{42} mode as the correction factor ($Q_{13} = Q_{13}^{TH} Q_{42}^{EX} / Q_{42}^{TH}$). With these data, we can calculate a_w using eqn.1. The data are summarized in Table 4. The error bar in a_w is due to estimated error in Q_{ohm}.

5. Conclusion

In these experiments, we have successfully generated an intense standing wave electromagnetic field using a gyrotron. The gyrotron interaction region and the FEL interaction region are contained within a single resonant cavity with a very high diffractive Q. The reason for high Q_d is to trap the RF power generated by the gyrotron interaction to build up the field in the standing wave (FEL) region. To achieve reasonable efficiency with a high Q_d cavity, we shortened the gyrotron interaction length considerably compared with

conventional gyrotron cavity designs. This also reduces the possible onset of the automodulation instability at high field amplitude [26]. A small portion of the RF signal is allowed to leak out for measurement. In addition, the total Q of the cavity is also measured in cold testing. The normalized wiggler field strength obtained is $a_w = 0.0057$, as compared to the theoretical value of 0.0098. The discrepancy can be due to a number of factors including resistivity of copper, mode conversion, velocity spread in the gyrotron beam,etc. Although the value of a_w achieved is quite small, larger values of a_w can be obtained with similar cavity design and higher power MIG guns. At present, an experiment is planned using a 85 kV, 35 A electron gun [27]. In such an experiment, a TE_{16}, 140 GHz, $a_w = 0.049$ wiggler field appears feasible. In short, we have demonstrated the operational principle of generating an intense standing wave field using a gyrotron. Such a field can be used as wiggler for compact FELs.

References

[1] Y.Carmel, V.L. Granatstein, and A. Grover, "Demonstration of Two-stage Backward-wave-oscillator Free Electron Laser," Phys.Rev.Lett., vol.51, pp.566-569, 1983.

[2] L.R. Elias, "High Power, Efficient, Tunable(uv through ir) Free Electron Laser Using Low Energy Electron Beams," Phys. Rev. Lett., Vol.42,pp.977-980,1979.

[3] V.L. Bratman, G.G. Denisov, N.S. Ginzburg, A.V. Smorgonsky, S.D. Korovin, S.D. Polevin, V.V. Rostov, and M.I. Yalandin, "Stimulated Scattering of Waves in Microwave Generators with high-current relativistic electron beams: Simulation of two-stage Free Electron Lasers," Int.J.Electron.,vol.59,pp. 247-289, 1985.

[4] S.Von Laven, S.B. Segall, and J.F. Ward,"A Low Loss Quasioptical Cavity for a Two Stage Free Electron Laser (FEL)", Proc.Free Electron Generators of Coherent Radiation, June 26-July 1, 1983, Proc. SPIE, vol.453, pp.244-254, 1983.

[5] H.R. Hiddlestone, S.B. Segall, and G.C. Catella, "Gain Enhanced Free Electron Laser with an Electromagnetic Pump Field", Physics of Quantum Electronics,vol.9, Reading, MA: Addison-Wesley, pp.849-865, 1982.

[6] J.S. Wurtele, G. Bekefi, B.G. Danly, R.C. Davidson, and R.J. Temkin, "Gyrotron Electromagnetic Wiggler for FEL Application," Bull.Amer.Phys.Soc., vol.30,p.1540,1985.

[7] B.G. Danly, G. Bekefi, R.C. Davidsion, R.J. Temkin, T.M. Tran, and J.S. Wurtele, "Principle of Gyrotron Powered Electromagnetic Wigglers for Free-Electron Lasers," IEEE J. Quantum Electron.,vol.QE-23, pp.103-116, 1987.

[8] T.M. Tran, B.G. Danly, and J.S. Wurtele, "Free-Electron Lasers with Electromagnetic Standing Wave Wigglers", IEEE J. Quantum Electron.,vol.QE-23, pp.1578-1589, 1987.

[9] J.S. Fraser, R.L. Sheffield, E.R.Gray, P.M.Giles, R.W.Springer and V.A.Loebs, "Photocathodes in Accelerator Applications", Proceedings of the 1987 IEEE Particle Accelerator Conference, Vol.3, pp.1705-1709.

[10] S.V. Benson, J.Schultz, B.A. Hooper, R. Crane and J.M.J.Madey, "Status Report on the Stanford Mark III Infrared Free-Electron Laser", Proceeding of the Ninth International FEL Conference.

[11] K.E. Kreischer and R.J. Temkin,"Single-Mode Operation of a High-Power, Step-

Tunable Gyrotron", Phys.Rev.Lett., vol.59, no.5, pp.547-550, 1987.

[12] P.Sprangle, C.M. Tang, and P. Sarafim, "Induced Resonance Electron Cyclotron (IREC) Quasi-Optical Maser", NRL Memorandum Report 5678.

[13] B.G. Danly, K.D. Pendergast, R.J. Temkin, and J.A. Davies, "Theory and Design of a High-Power, 140 GHz CARM Amplifier," Proc. S.P.I.E., vol.873, pp.143-147, 1988.

[14] K. Felch, D. Stone, H. Jory, R. Garcia, G. Wendell, R.J. Temkin, and K.E. Kreischer, "Design and Operation of Magnetron Injection Guns for a 140 GHz Gyrotron," IEDM Technical Digest, 14.1, 362-365, 1982.

[15] K.E. Kreischer, and R.J. Temkin, "High Frequency Gyrotron and Their Applications to Tokamak Plasma Heating," Infrared and Millimeter Waves, vol.7, pp.377-485, 1983.

[16] B.G. Danly, and R.J. Temkin, "Generalized Nonlinear Harmonic Gyrotron Theory," Phys.Fluids, vol.29, pp.561-567, 1986.

[17] V.L. Bratman, N.S. Ginzburg, G.S. Nusinovich, M.I. Petelin, and P.S. Strelkov, "Relativistic Gyrotrons and Cyclotron Autoresonance Maser," Int.J.Electron., vol.51, pp.541-567, 1981.

[18] G.S. Nusinovich and R.E. Erm, Elektron.Tekh.,Ser.1, Elektron. SVCh, 55 (1972).

[19] A.W. Fliflet, M.E. Read, "Use of Weakly Irregular Waveguide Theory to Calculate Eigenfrequencies, Q Values, and RF Field functions for Gyrotron Oscillators," Int.J.Electron., vol.51, pp.475-484, 1981.

[20] K.E. Kreischer, J.B. Schutkeker, B.G. Danly, W.J.Mulligan, and R.J. Temkin, "High Efficiency Operation of a 140 GHz Pulse Gyrotron", Int.J.Electronics, vol.57, No.6, pp.835-850, 1984.

[21] K.E. Kreischer, B.G. Danly, P.Woskoboinikow, W.J. Mulligan, and R.J.Temkin,"Frequency Pulling and Bandwidth Measurements of a 140 GHz Pulsed Gyrotron", Int. J. Electronics, Vol.57, No.6, pp.851-862,1984.

[22] H.R. Fetterman, P.E. Tannenwald, C.D. Parker, J. Melngalis, and R.C. Williamson, P. Woskoboinikow, H.C. Praddaude, and W.J. Mulligan, "Real-time Spectral Analysis of Far-Infrared Laser Pulses Using a SAW Dispersive Delay Line," Appl.Phys.Lett., vol.34, pp.123-125, 1979.

[23] K.E. Kreischer and R.J. Temkin, "Linear Theory of an Electron Cyclotron Maser

Operating at the Fundamental," Int.J.Infrared Millimeter Waves, vol.1, pp.195-223, 1980.

[24] L.J. Chu, "Calculation of the Radiation Properties of Hollow Pipes and Horns", J.App.Phys., vol.11, pp.603-610, 1940.

[25] P.P. Woskoboinikow, and W.J. Mulligan, "Nondestructive Gyrotron Cold-Cavity Q Measurements",IEEE Trans. MTT, vol.35,no.2, pp.96-100, 1987.

[26] G.S. Nusinovich and E.M. Sher, "Theory of Non-stationary Processes in Cyclotron Resonance Masers with Counterrunning Waves", Int.J.Electronics, vol.56. no.3, pp.275-286, 1984.

[27] K.E. Kreischer, B.G. Danly, J.B. Schutkeker, and R.J. Temkin, "The Design of Megawatt Gyrotron," IEEE Trans. Plasma Sci., vol.PS-13, pp.364-373, 1985.

Table 1 Comparison of EM Wiggler with MS Wiggler

a_w	λ (cm) EM wiggler	B_w (G)	λ_w (cm) MS wiggler	B_w(G) helical	B_w(G) planar
0.008	0.23	374	0.115	748	1058
0.049	0.23	2290	0.115	4580	6477

Table 2 Design Parameter Values

Mode	TE_{13}
Q_D	84200
Q_{ohm}	43600
Q_{tot}	28700
F(Gyrotron)	0.3
μ (Gyrotron)	7.0
$k_{\|}/k$ (FEL)	0.9
a_w (FEL)	0.0098

Table 3 Mode Identification

mode	measured frequency (GHz)	Calculated frequency
TE_{32}	121.596	121.342
TE_{13}	129.510	129.169
–	134.130	–
TE_{81}	145.645	145.961
TE_{23}	151.124	151.391
TE_{03}	154.569	155.072
TE_{52}	159.550	160.112

Table 4 130 GHz GEM Wiggler Results

Parameter	Experimental Value	Designed Value
I	4.25 A	5 A
ν	129.560 GHz	129.168 GHz
Q_T	26800	28700
Q_D		84200
Q_{ohm}		43600
P_D	11.2 kW	31.1 kW
P_{ohm}	21.6 kW	60.1 kW
a_w	0.0057 ± 0.0006	0.0098

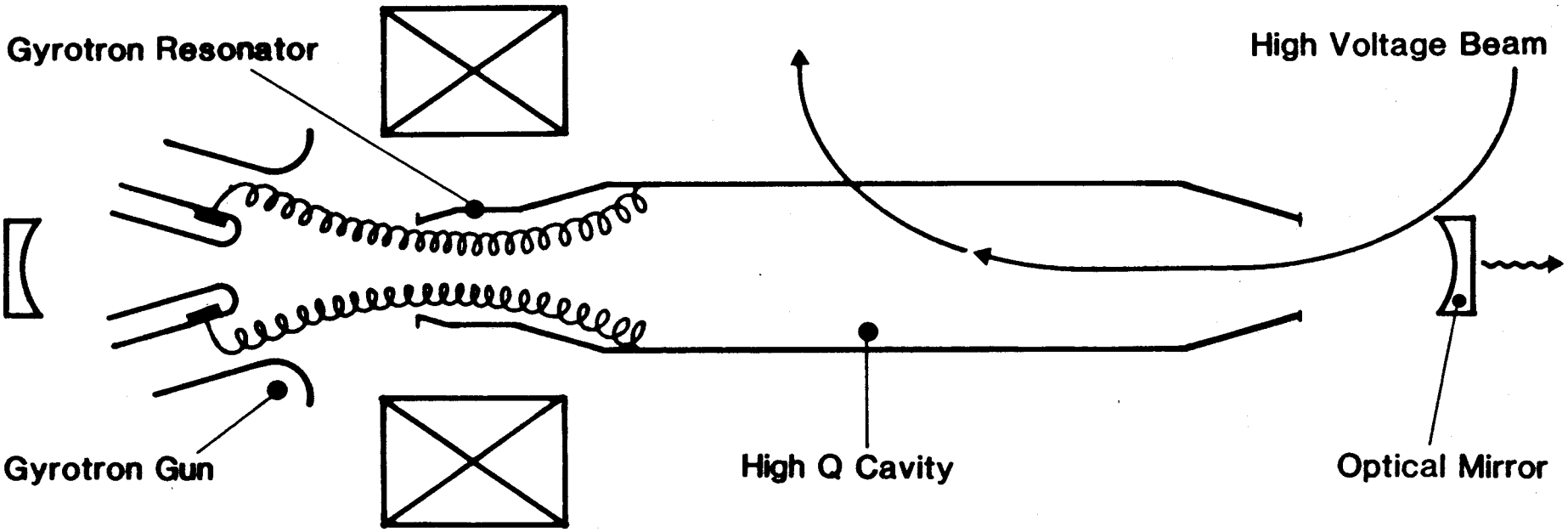

Fig.1 Schematic Diagram of the Standing Wave GEM Wiggler FEL Configuration

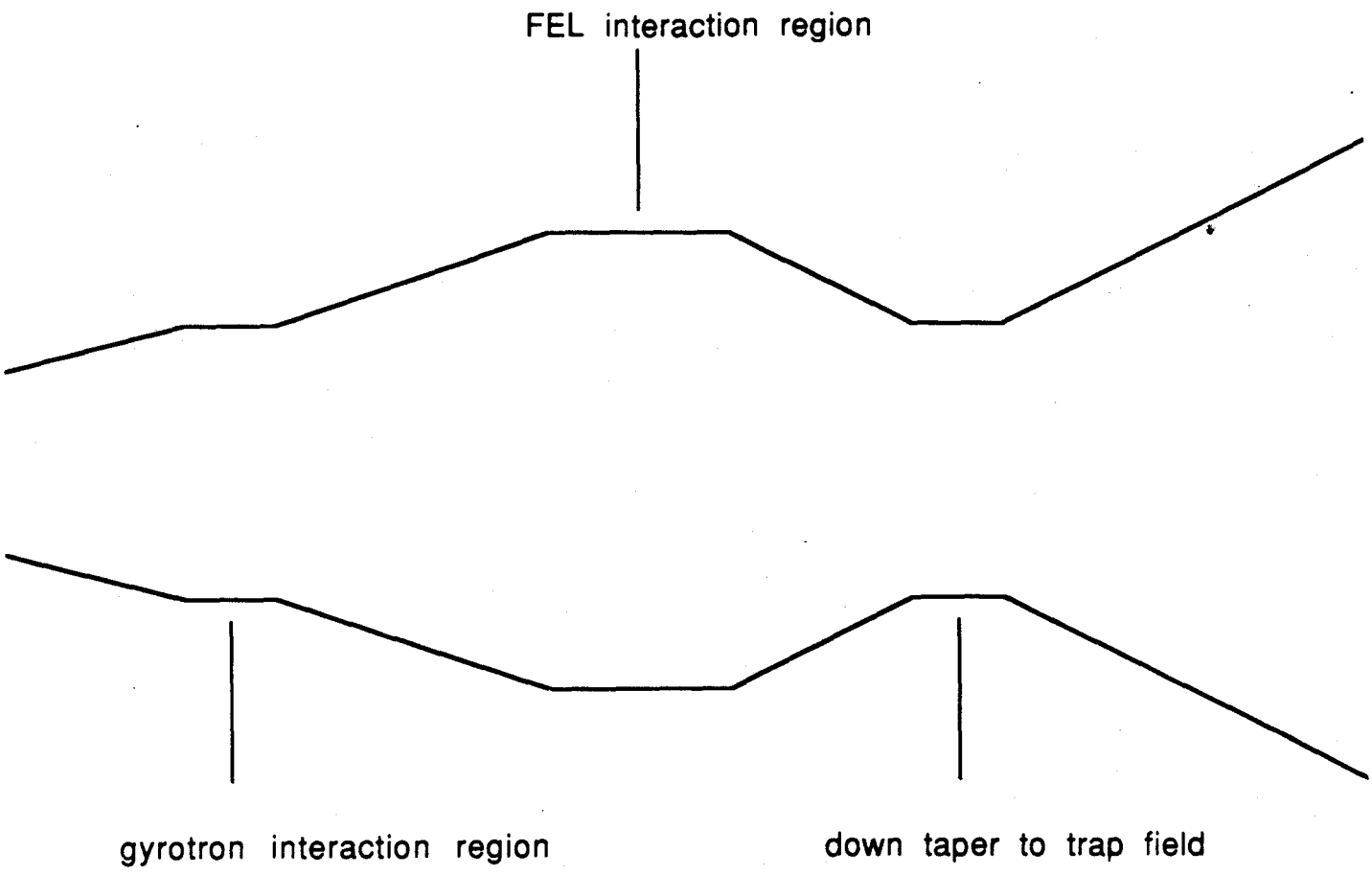

Fig.2 Schematic Diagram of the GEM Wiggler Cavity

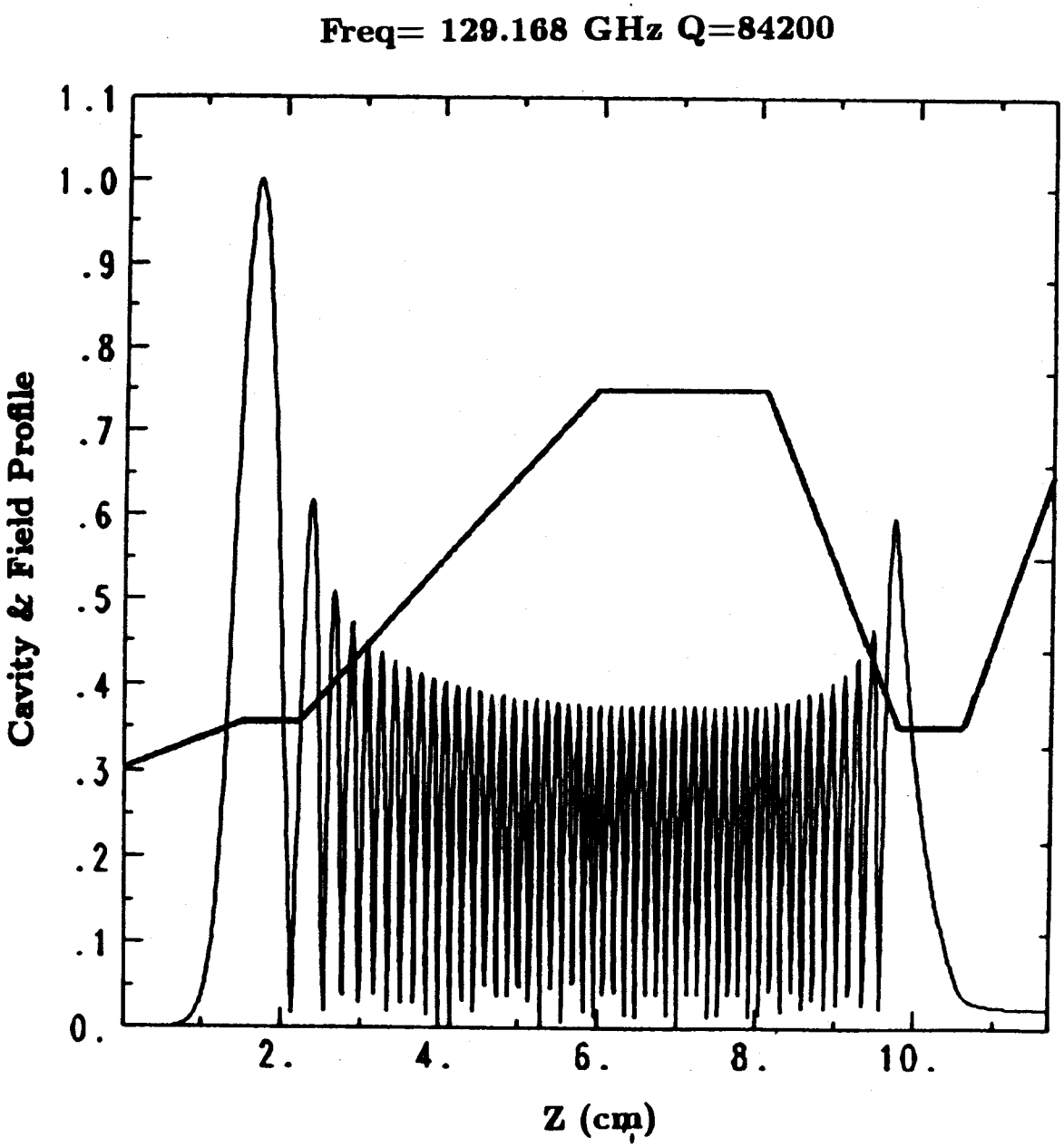

Fig.3 Axial Field Profile Inside the Cavity Calculated by CAVRF

Fig.4 A Picture of the GEM Wiggler Cavity

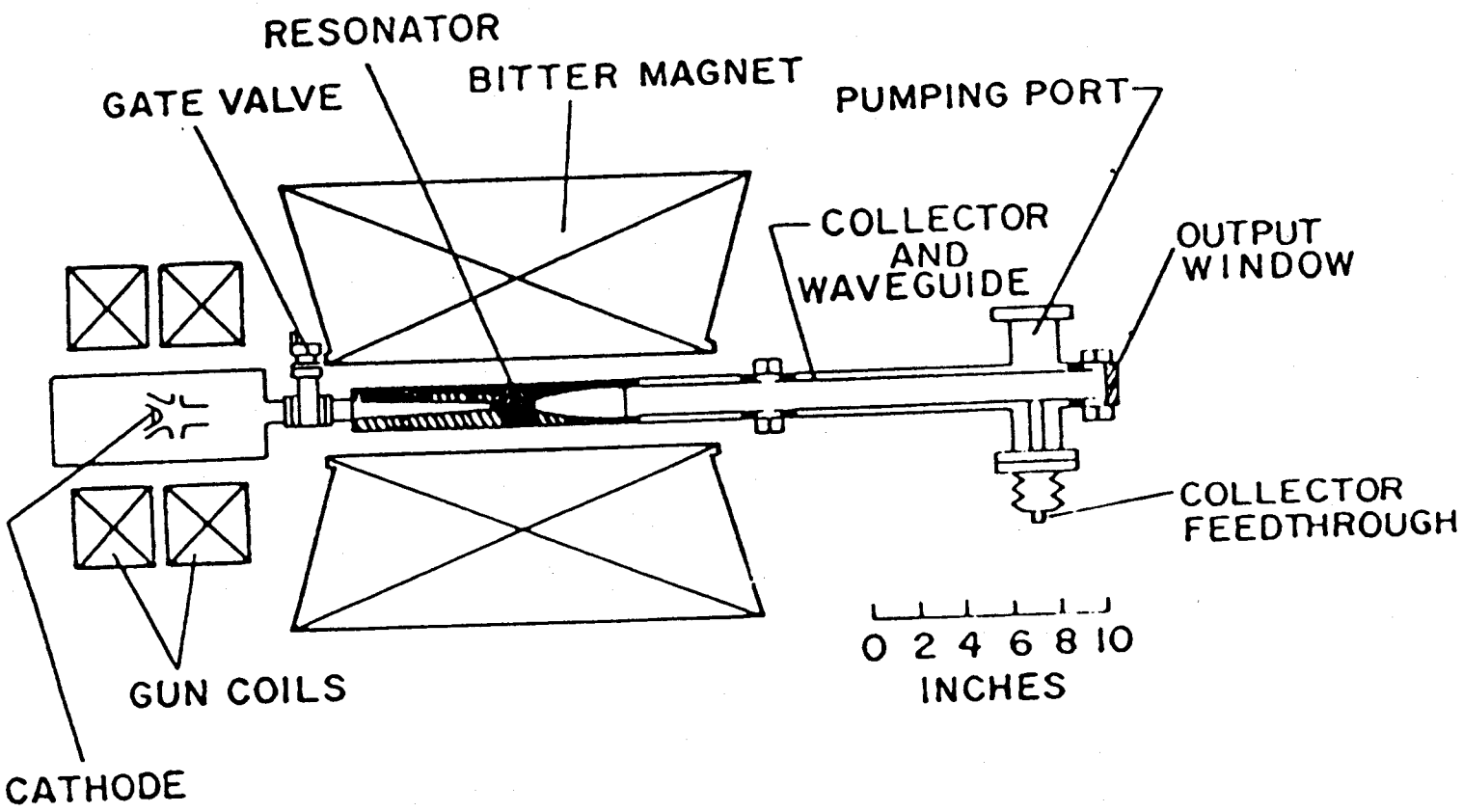

Fig.5 Schematic Diagram of the Experiment Setup

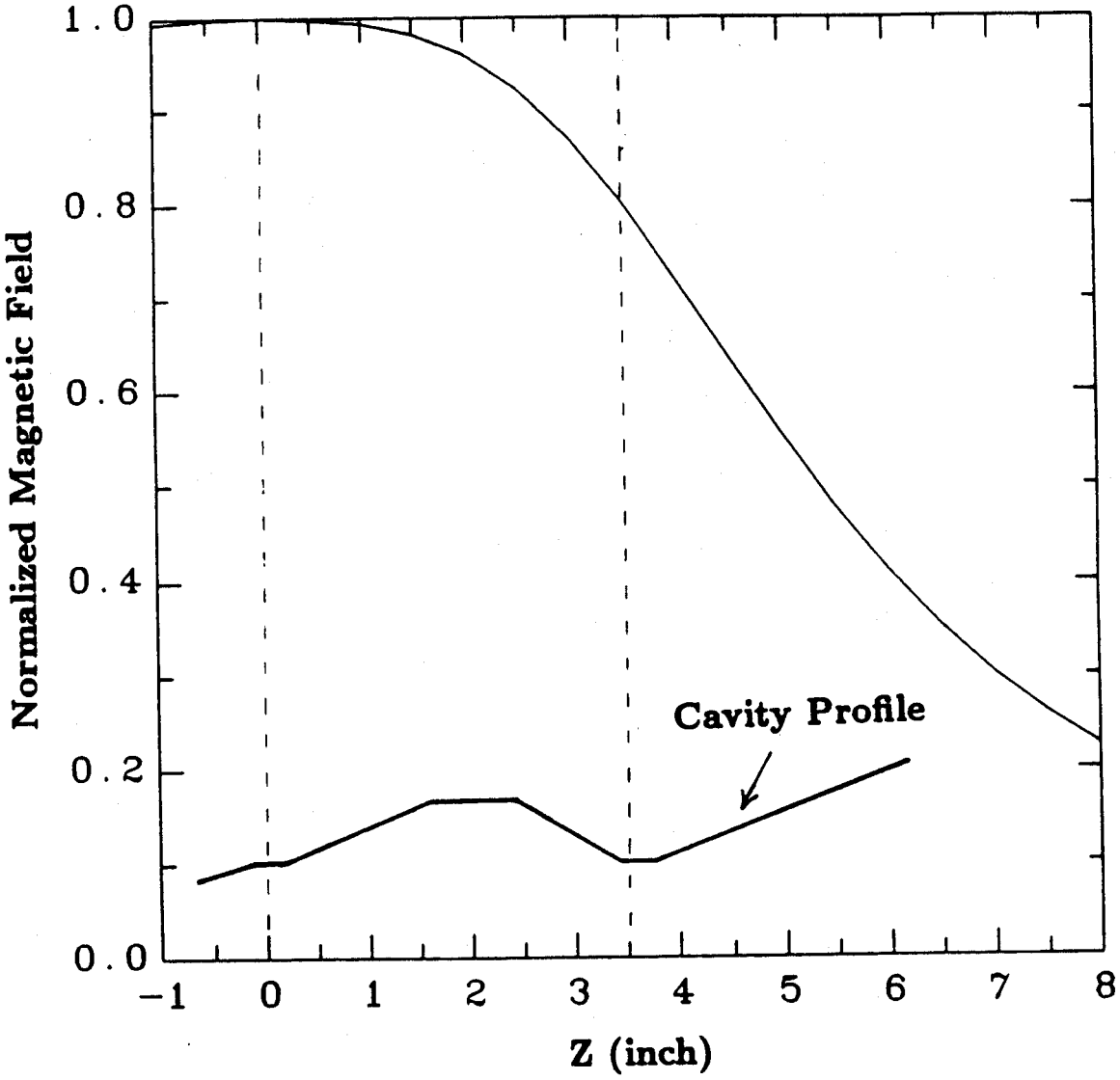

Fig.6 Magnetic Field Profile over the Entire Cavity

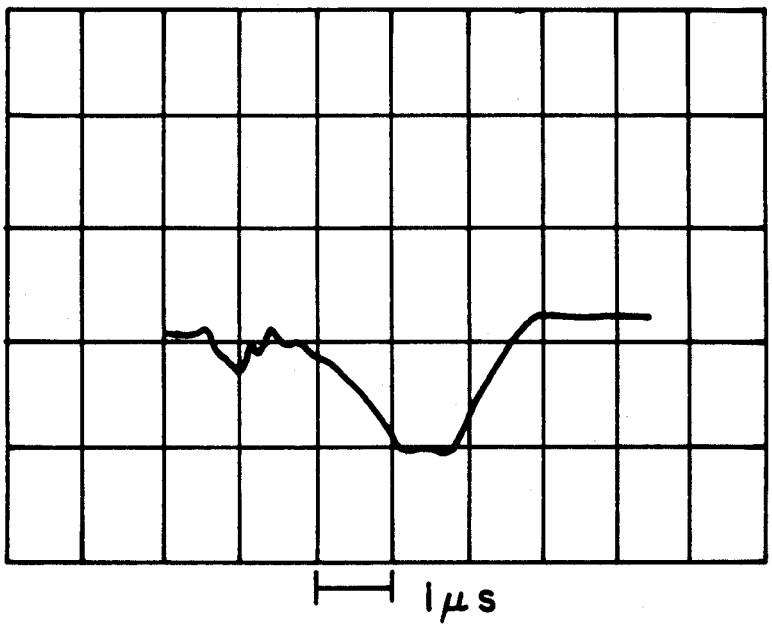

Fig.7 Diode Signal of the TE_{13} Mode

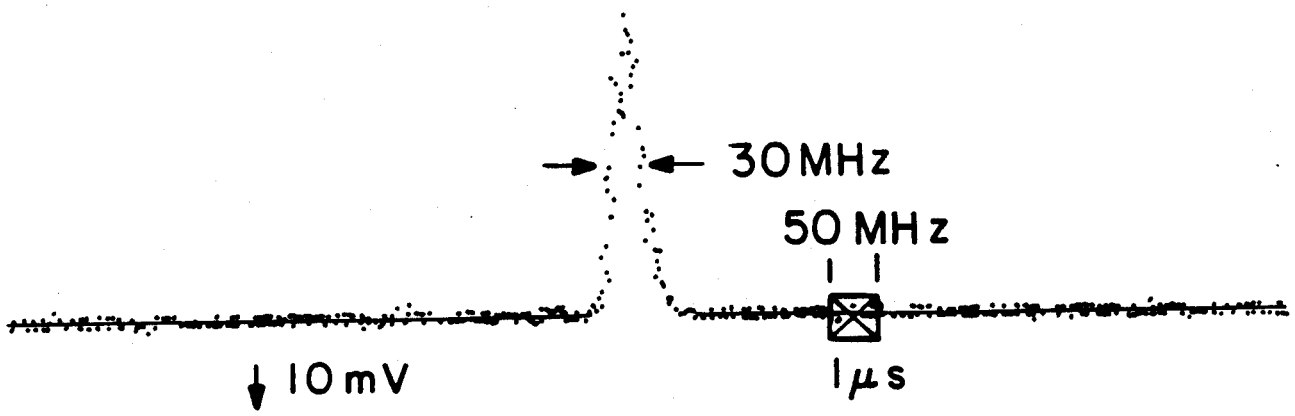

SAW Signal

Fig.8 SAW Signal of the TE_{13} Mode

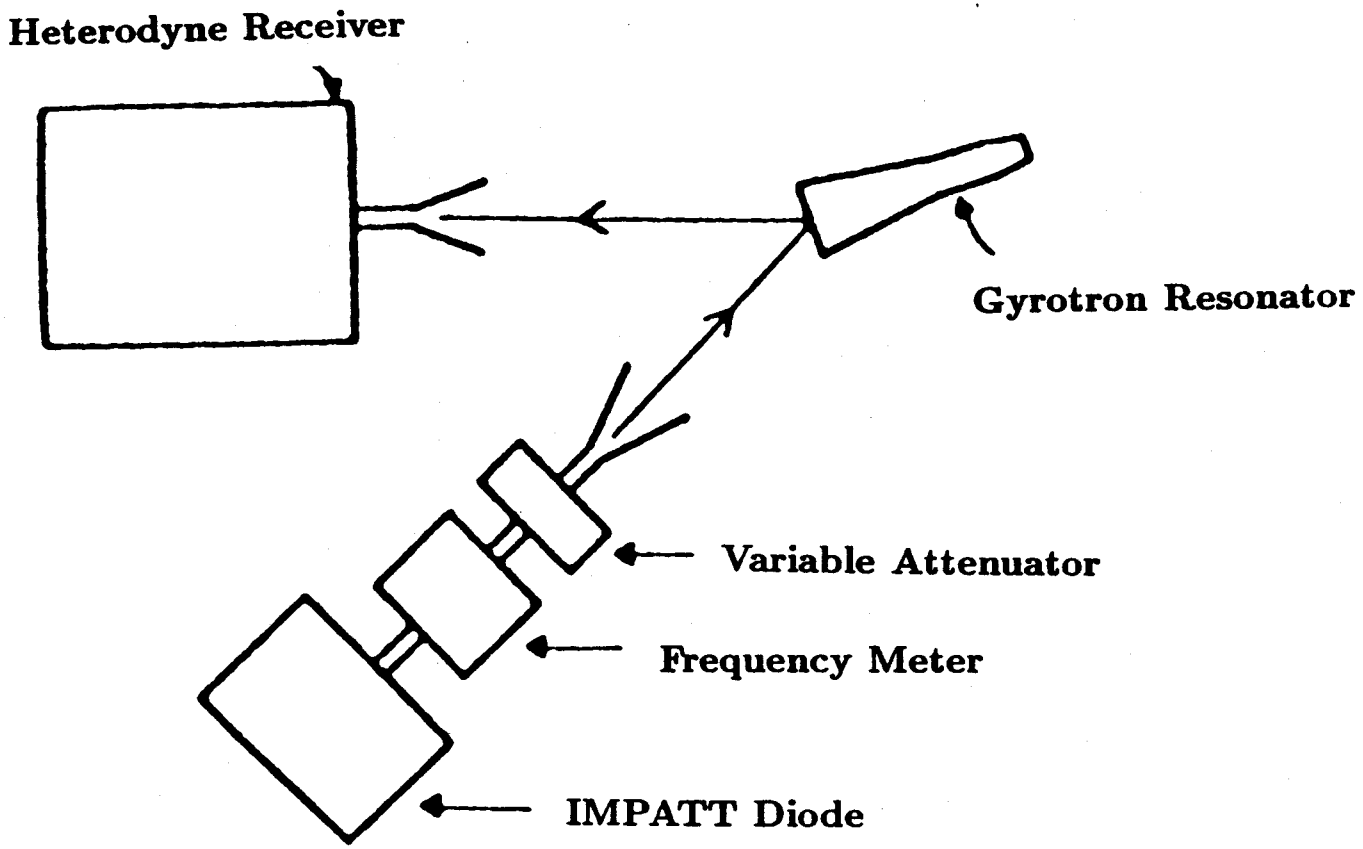

Fig.9 Experimental Setup for Measuring the Cold Cavity Q